Title
REALISTIC NUCLEAR SINGLE-PARTICLE HAMILTONIANS AND THE PROTON SHELL 114

Author
Meldner, Heiner.

Publication Date
1968-12-01

UCRL-17801

cy. 2

REALISTIC NUCLEAR SINGLE-PARTICLE HAMILTONIANS AND THE PROTON SHELL 114

Heiner Meldner

October 1968

LAWRENCE RADIATION LABORATORY
UNIVERSITY of CALIFORNIA BERKELEY

UCRL-17801

DISCLAIMER

Submitted to Physical Review

UCRL-17801
Preprint

UNIVERSITY OF CALIFORNIA
Lawrence Radiation Laboratory
Berkeley, California

AEC Contract No. W-7405-eng-48

REALISTIC NUCLEAR SINGLE-PARTICLE HAMILTONIANS AND THE PROTON SHELL 114

Heiner Meldner*

(revised October 1968)

REALISTIC NUCLEAR SINGLE-PARTICLE HAMILTONIANS AND THE PROTON SHELL 114

Contents

REALISTIC NUCLEAR SINGLE-PARTICLE HAMILTONIANS AND THE PROTON SHELL 114[+]

Heiner Meldner[x]

Lawrence Radiation Laboratory and Department of Physics
University of California
Berkeley, California

ABSTRACT

A simple selfconsistent single-particle equation is investigated and compared with similar attempts. The proposed model is designed to be particularly suitable for the calculation of (adiabatic) fission processes. The kernel of this integro-differential equation has a structure that allows to reproduce satisfactorily with one constant set of five physical parameters

1) charge density distributions, including isotope shifts,
2) 1 s proton levels as measured in (e, e'p) scattering,
3) total binding energies or nuclear mass defects, and
4) the shell model spin assignments and mass structure

throughout the periodic table. Hence, it seems that all future work in this direction has to confirm quantitatively the essential features determined here; in particular the nonlocality and rearrangement effects. Rearrangement

energies appear explicitly, since the present model, similar to self-consistent fields of appropriate many-body formalisms, yields different eigenvalue spectra and mass defects for different occupation functions. The partial derivative $\partial E / \partial Z$ of the total binding energy (mass) changes considerably at the proton number $Z = 114$ when the present Hamiltonian is used for super-heavy nuclei. This confirms an earlier suggestion made by this author on the basis of a gap in the proton eigenvalue spectrum at $Z = 114$. The present calculations show this shell effect to become insignificant for isotopes too far from the extrapolated beta stability line, in particular for $N \lesssim 172$.

INTRODUCTION

Phenomenologically, the Hamiltonian for a nucleon bound in a nucleus allows a rapidly converging expansion: H = H1 + H2 + ... in terms of one-body, two-body, etc. operators; i.e. a "realistic" model for the single-particle Hamiltonian H1 accounts rather accurately for gross nuclear data of bound and scattering states - thus leaving only small phenomenological many-body forces to produce residual correlations. This picture comprehends essential facts like the pronounced nuclear shell structure and the extremely small ratio of the odd-even mass staggerings to the nuclear binding energies. However, even a dozen years after the establishment of the shell model phenomenology [1-3], basic quantitative questions, e.g. about the extent of nonlocality of H1 and it's rearrangement - type response are far from being noncontroversially settled.

One purpose of this work is to investigate such features of realistic nuclear single-particle Hamiltonians without the usual strong restrictions and oversimplifications due to rather limited computer facilities. For example, self-consistent equations with nonlocal potentials are solved (numerically) exactly here.

Two approaches for the determination of H1 are easily distinguished: Number one is the direct pragmatic way, i.e. an ansatz for a phenomenological single particle equation (usually involving nonlocal one-body potentials). Number two deploys some many-body formalism with phenomenological two-body potentials. At the present stage of the theory , preference of the latter is unfortunately based on the prejudice that a complicated answer to a complicated question is more reliable than a simple one. This uncertainty is due to the fact that all number two approaches - although potentially closer to a first principle method - still have to be based on a practically unsolved many-hadron problem.

The NN interaction is not sufficiently understood at the distances of major importance for this purpose, i.e. smaller than half the inverse pion mass [4]. This implies the high uncertainty about the off energy shell behaviour of NN potentials [5] - in particular about their nonlocality. The latter quite obviously exhibits the ambiguity of fits of the two-body NN scattering with potential models; since one can always construct classes of phase shift equivalent potentials with identical spectra but quite different off energy shell behaviour, including cases which give singular Hartree-Fock-type matrix elements. E.g. any unitary transformation acting on a given two-body Hamiltonian that contains some NN phase shift fitting potential gives another Hamiltonian, say $e^{i\Omega} H e^{-i\Omega}$, with a potential of generally different nonlocality of off energy shell behaviour. The fit to the on shell data is preserved, as long as the change of the T-matrix (proportional to the change of the Hamiltonian [6]) vanishes there, i.e. $\delta T \sim \delta H \sim [\Omega, H] = 0$. Thus, all such transformations with hermitian two-body operators Ω yield equivalent on shell potentials, once the transition matrix element of this commutator vanishes [7]. This can be viewed as a formal method to obtain families of equivalent potentials by generalized Scott-Moszkowski-type [8] separations. Therefore, it would seem futile to work numerically with approach number two, as long as the question of off energy shell behaviour is not sufficiently understood <u>quantitatively</u>. Presently, it is hardly possible to decide here <u>qualitatively</u>, namely between the extreme cases of purely local hard core versus highly nonlocal smooth potentials [9].

Safe, however, seems the basis of a nonrelativistic potential description of NN forces at the low kinetic energies of nucleons bound in many-baryon systems. This belief is due to the small ratio of the pion to the nucleon mass [10]. Thus, it is also safe to rely on the gross

structure of single particle equations as given by many-body formalisms and approximations which are based on sufficiently general NN potentials. This - presently wise - restriction to the qualitative results of such formalisms requires the parametrization of a nuclear single-particle Hamiltonian, as is done e.g. via the ansatz of a Woods-Saxon or Nilsson-type potential; usually with some velocity dependence [11-14]. However, these simple models of a nuclear self-consistent field can be replaced now. Modern computers allow a considerably improved simulation of the nuclear single-particle equations that are expected from reasonable many-body formalisms.

One suggestion in this direction is made here (Sect. 1). Actual complications in comparison to the ancient nuclear well ansatz were found to be unnecessary. The proposed single particle Hamiltonian has a structure close to the one given grossly by Hartree-Fock-Bogolubov or Brueckner-type formalisms. I.e. nonlocality, density-, spin-orbit-, and i-spin-dependences are introduced into the kernel of this equation in a form as expected in first order from such formalisms involving rather general nonlocal NN potentials.

Sect. 2.2 shows that only five physical parameters allow a surprisingly good fit to many independent data throughout the periodic table. Such a widespread application was inconceivable with previous models of H1. The essential features of a realistic single-particle Hamiltonian seem to be determined rather uniquely this way. They will have to be confirmed, once substantial experimental information on the off energy shell behaviour of NN potentials has been accumulated so that some number two approaches can leave the status of model-dependent models. The quantitative results of the fairly conservative and pragmatic approach adopted here provide a rather safe foundation. This resembles the situation in nuclear physics of small baryon number hadron systems, where a pragmatic approach now

determines basic features in terms of Regge singularity parameters.

Rearrangement-type responses (Sect. 3) of this self-consistent model appear to have the right order of magnitude. Orbital rearrangement energies, for example, were found to be comparable to level spacings in nuclear potential wells.[15] This result seriously questions the usual identification of such level spacings with the mass differences observed e.g. in nucleon transfer reactions.

In the presence of fluctuating rearrangement energies, a gap in the eigenvalue spectrum, as e.g. found at the proton number 114, does not necessarily lead to a real shell effect in the masses as a function of nucleon numbers. The deployment of this realistic Hamiltonian in the region of super-heavy nuclei (Sect. 4) therefore provides an almost independent check on the magic proton number 114 which was originally[13, 14, 16-18] suggested from extrapolations of proton eigenvalue spectra.

All data in this paper refer to spherical nuclei; Sect. 5 deals in some detail with the straightforward extension of this self-consistent field model to axially symmetric deformed densities. The present form has particular advantage for the description of adiabatic fission processes.

The appendices are concerned with some of the computational problems.

1. The Self-Consistent Field Model

A single-particle equation of the type

$$\left(\frac{\hbar^2}{2m}\frac{\partial^2}{\partial\vec{r}^2} - \varepsilon_{\nu,m_t}\right)\varphi_{\nu,m_t}(\vec{r}) = \int d\vec{r}'\, K_{m_t}(\vec{r},\vec{r}')\,\varphi_{\nu,m_t} \qquad (1)$$

is sufficiently general to allow for a rather realistic model of the nuclear self-consistent field. The subscript ν stands for all quantum numbers specifying a bound nucleon except for its i-spin 3-component m_t. The deployment of plain Hartree Fock, for instance, i.e.

$$K^{HF}_{m_t}(\vec{r},\vec{r}') = \sum_i \left(\varphi_i^*(\vec{r})\,u(\vec{r},\vec{r}')\,\varphi_i(\vec{r}') - \delta(\vec{r}-\vec{r}')\int d\vec{r}\,\varphi_i^*(\vec{r})\,u(\vec{r},\vec{r}')\,\varphi_i(\vec{r}')\right) + \left(\tfrac{1}{2}-m_t\right)K_{Coulomb} \qquad (2)$$

with suitable models for $u(r, r')$ provides nuclear single-particle Hamiltonians which are quantitatively almost as useful as the ones mentioned in the introduction [19]. Therefore HF, i.e. the result in the limit where perturbation methods are applicable to more general many-body formalisms is sometimes referred to in the following discussion - although one should by no means regard the phenomenological kernel proposed here as being necessarily connected with a plain HF formalism.

A comparison of (2) with the symmetrical factorized Van Vleck-type kernel [20]

$$K_{m_t}(\vec{r},\vec{r}') = v(|\vec{r}-\vec{r}'|)\cdot u_{m_t}(\vec{r}+\vec{r}') + \left(\tfrac{1}{2}-m_t\right)K_{Coulomb} \qquad (3)$$

yields upper bound estimates for the "ranges" of u and v. Namely the range in $|r - r'|$ should not exceed the order of the inverse pion mass (1.4fm) and the function u should essentially vanish for its argument larger than nuclear radii ($A^{1/3}$fm). Therefore u is usually taken to be proportional to the nuclear matter distribution. Lower limits on the range of the factor v are, for instance, required in order to reproduce the observed momentum dependence of local potential wells, i.e. the fact that the effective mass of bound nucleons is not larger than 0.5 in real nuclei [3,21]. As is shown in the next section, this clearly excludes nonlocality ranges which are small enough to render a δ-function for v, i.e. local potentials a reasonable ansatz. Since the factorized form (3) also allows for selfconsistency, it would appear to yield the simplest kernel that has a chance to simulate any realistic nuclear self-consistent field.

1.1 Nonlocality

Fig. 1 accumulates empirical information on the Fourier transform of $v(|r - r'|)$. I.e. the approximately equivalent (momentum)^2 dependent local potential depth $\tilde{v}(k^2)$, defined e.g. through

$$\varphi\tilde{v}(k^2) = \int d\vec{r}' K(\vec{r},\vec{r}')\varphi(\vec{r}') = \varphi u(0)\int d\vec{r}' e^{i\vec{k}\cdot(\vec{r}-\vec{r}')} v(|\vec{r}-\vec{r}'|) \qquad (4)$$

Therefore, in order to specify reasonably well a nonlocality function $v(|r - r'|)$, one needs in addition to its width in $|r - r'|$ at least one more property like its asymptotic slope. For example, Yukawa and

Gaussian formfactors $v(|r - r'|)$ fit the dashed curve in fig. 1

$$v_o(\varepsilon) = v(\varepsilon - v_o(\varepsilon)) \tag{5}$$

with widths around 0.8 and 1.5 fm respectively (cf. ref. 14). The most important evidence on $v_o(\varepsilon)$ in region 1 comes from the (e, e'p) experiments [22]. The data on ^{40}Ca and ^{75}As suggest that 1s protons are bound by at least 80 MeV in heavier nuclei. Other limits on $v_o(\varepsilon)$ in this region may be inferred from estimates of the effective nucleon mass in nuclear matter [3, 21].

In region 2, i.e. for ε around the Fermi energies, $v_o(\varepsilon)$ is most accurately determined in absolute magnitude - via the observed separation energies. But the slope there is subject to quite some speculation . One school suspects an appreciable wiggle there [23], a zero or even sign change of the slope as indicated by the dotted line in fig. 1. However, the arguments presented for such anomalies are not conclusive yet (cf. Sect. 3 and ref. 15).

In region 3 and 4 the evidence comes mainly from fits of nucleon-nucleus scattering [24-28]. Although one cannot completely disentangle the energy dependencesof real and imaginary parts, there is general agreement now that the real part has the minimum decrease with energy indicated in fig. 1 for the well analyzed 10 MeV region. Straightforward use of the real part of an optical model fit did exactly yield the shell structure [11]. However, the nonlocality there did correspond to the lower limit for the slope indicated in region 3 (derived from refs. 25, 26) and gave only about half the total binding energy [29]. Therefore, the stronger energy dependence indicated by other optical model fits [27]

is favoured from the bound state fits - if one excludes a strong curvature of $v_o(E)$ for $E \lesssim 0$. No appreciable energy dependence is established for the 100 MeV region; v_o may essentially become a constant there[24, 28].

The dashed curve in fig. 1 corresponds to a Yukawa nonlocality function with the width used here (cf. set A of table 1). This simple form can account quite well for the data. Superpositions of several Yukawas that did, for instance, give a wiggle in region 2 were found to be unnecessary at this stage of the phenomenology. A Yukawa, i.e. a NN potential-type function is suggested from the Van Vleck kernel and seems to fit the curvature in fig. 1 a little better than a Gaussian.

1.2 Saturation and Density Dependence

The real part of u in Van Vleck-type kernels is usually taken to be similar to the matter density ρ.[20, 25] Taking literally $u = \rho\left(\frac{\vec{r}+\vec{r}'}{2}\right)$ is, of course, not consistent: The output ρ from a bound state calculation has a smaller rms radius than the input. This self-consistency problem can be solved by adding to the width function v , the "interaction" in the Van Vleck kernel some density dependence like

$$V(\vec{r}-\vec{r}')\left[1 - \alpha\,\rho^{\beta}\left(\frac{\vec{r}+\vec{r}'}{2}\right) - \cdots\right] \qquad (6)$$

with α, $\beta > 0$. The resulting kernel $\sim v \cdot (1 - \alpha \rho^{\beta})$ gives a sum of terms proportional to $\rho^{\frac{2}{3}}$, $-\rho$, and $\rho^{1+\beta}$ for the energy - readily seen from the Thomas-Fermi approximation. One can therefore get it stationary at the observed nuclear saturation densities. In this class is, for instance, Bethe's recent proposal for the effective NN interaction [30]: $v \cdot (1 - \alpha \rho^{\frac{2}{3}})$. A similar term appears in HF-type formalisms as a first order correction for nonlocality of the two-body potential. This is seen from the analogous formula to eq. (4) for a nonlocal NN potential. The equivalent momentum dependent potential derived this way is a local one multiplied by the usual power series in momentum operators squared - if the kernel is symmetric:

$$v \cdot (1 - ap^2 - bp^4 - \ldots) \qquad (7)$$

And eq. (6) follows from the statistical approximation:
The particular power $\beta = \frac{2}{3}$ is therefore suggested from such considerations and used in the model below. The choice is not critical as long as it is not very different from this value: Some variations in the range $0.3 \leq \beta \leq 1$ with adjustments of other parameters left results practically unchanged.

Similar arguments hold for the simplification of taking $\rho\left(\frac{|\vec{r}|+|\vec{r}'|}{2}\right)$ instead of $\rho\left(\frac{\vec{r}+\vec{r}'}{2}\right) = \rho\left(\frac{|\vec{r}+\vec{r}'|}{2}\right)$ for the spherical density distributions considered here (for nonspherical ρ see sect. 5). Both choices should give essentially the same fits to the data up to some parameter renormalization.

A summation of the preceding considerations therefore yields as the most straightforward model of a nuclear kernel:

$$K(\vec{r},\vec{r}') = v(|\vec{r}-\vec{r}'|) \cdot \left[1 - \left(\frac{\rho(x)}{\rho_1}\right)^{\frac{2}{3}}\right] \cdot \rho(x), \qquad x = \frac{|\vec{r}|+|\vec{r}'|}{2} \qquad (8)$$

This will be adorned by two "fine structure" terms discussed in the following subsections.

1.3 I-Spin Dependence

Conventionally, the i-spin dependence of nuclear single-particle Hamiltonians is introduced via a Lane potential [31]

$$\vec{t} \cdot \vec{T}/A \tag{9}$$

where $\vec{t}$ and $\vec{T}$ are respectively the i-spins of the nucleon and residual nucleus in question. However, this term yields the wrong isotopic variation of rms radii of e.g. Ca isotopes if it is used with the strength necessary in optical model fits or as required to fit the neutron/proton ratio in heavy nuclei. Only an inconsistently small strength parameter could reproduce the data [32].

Considerations similar to the ones that led to the kernel (8) would suggest to use for the effective ρ an appropriately weighted average of the densities $\rho_{(\pm\frac{1}{2})}$ corresponding to neutrons and protons, namely

$$\rho_{m_t} \sim \rho_{(-m_t)} + \tau \rho_{(m_t)} \tag{10}$$

with a dimensionless parameter $\tau < 1$. This can be interpreted as assuming that only a fraction of the like nucleons interact with the particle in question. or are felt by the particle as attractive as the unlike ones. One can therefore account for effects of the Pauli principle as well as for i-spin dependent terms in the NN interaction. It is only the latter that led to the assumption of the Lane potential. In the statistical limit, where surface terms are neglected, a simple exercise showsthe present ansatz (10) to be completely equivalent to Lane's term $\rho \cdot (1 + \alpha \vec{t} \cdot \vec{T}/A)$. However, eq. (10) can reproduce satisfactorily the neutron/proton ratios or optical model results as well as the isotope shifts in rms radii. Recent fine structure investigations of the i-spin dependence [33] also seem to favour a term like (10).

1.4 Spin-Orbit Interaction

A single-particle spin-orbit term of the type

$$\vec{s}\vec{\ell}\,\frac{1}{r}\frac{d\rho}{dr} \tag{11}$$

can be derived from HF-type formalisms [34] and now even its strength appears to be understood in this framework [35]. About equally satisfactory seems to be the pragmatic introduction of this term as the simplest invariant (with respect to rotations and inversions) proportional to $\vec{p}$, $\vec{s}$, and $\nabla\rho$, namely [36] $(\vec{p} \times \vec{s})\cdot\nabla\rho$. This gives eq. (11) for spherical nuclei. However, the present calculations with such a term did not show very clearly the shell structure for heavy nuclei, as seen e.g. from the results of the next section. One reason seems to be the factor $r^{-1}d\rho/dr$ that emphasizes the influence of wiggles in the inside density distribution. This did not show up in similar but non-self-consistent models where the density (or potential) was proportional to the usual Fermi function that is practically constant inside. Therefore, a form

$$r^2(\vec{p}\times\vec{s})\cdot\nabla\rho \tag{12}$$

might improve the results.

2.1 The Five Parameter Kernel

The accumulation of all essential pieces from sect. 1 yields the five parameter kernel

$$K_{m_t}(\vec{r},\vec{r}') = \frac{v\exp(-y/a)}{y/a}\left[1-\left(\frac{\rho_{m_t}(x)}{\rho_1}\right)^{\frac{2}{3}}\right]\left[1-\frac{\sigma}{x}\vec{S}\vec{l}\frac{d}{dx}\right]\rho_{m_t}(x) + \delta(y)\left[\tfrac{1}{2}-m_t\right]\cdot V_{Coul}(x), \tag{13}$$

with $$\rho_{m_t} = \left[\rho_{(-m_t)} + \tau\rho_{(m_t)}\right]\frac{1}{1+\tau}, \quad x = \frac{r+r'}{2}, \quad y = |\vec{r}-\vec{r}'|$$

and $$\rho_{(m_t)} = \sum_{\nu}^{\nu_{Fermi}} |\varphi_{\nu,m_t}|^2 \tag{14}$$

for the self-consistent field model (1) of spherical nuclei. The electromagnetic part is assumed to be given by the static Coulomb potential V_{Coul} of the proton density $\rho_{(-\frac{1}{2})}$ normalized to Z - 1; cf. (17).

1) The parameter v simply determines the energy scale and was adjusted in all computations to give (within 0.3 MeV) the total binding energy for Pb^{208}.

2) According to the discussion in sect. 1.2, the nonlocality range should be $0.7 \lesssim \frac{a}{fm} \lesssim 0.9$. An increase in a widens the level spacings, i.e. decreases the effective nucleon mass - as is readily seen from eqs. (4) and (5). An increased a yields larger rms radii if v is decreased according to 1) and all other parameters are kept fixed (cf. the discussion below on parameter set B).

3) The parameter ρ_1 stands for the (average) critical nucleon density where the nucleon-nucleus interaction changes from attractive to repulsive. Since actual nuclei saturate with (average) central densities around $0.15\ \mathrm{fm}^{-3}$, ρ_1 must be larger than this value. An upper limit around $0.5\ \mathrm{fm}^{-3}$ is given from hard sphere packing according to hard core NN potential models. It turns out that the present model reproduces the rms radii of actual nuclei for $0.2 < \frac{\rho_1}{\mathrm{fm}^{-3}} \lesssim 0.4$.

4) The observed sequence of shell closures allows a fairly unique determination of the strength σ for the conventional spin-orbit term. This parameter is confined here to $0.45 \lesssim \frac{\sigma}{\mathrm{fm}^2} \lesssim 0.55$ if one wants to reproduce the magic nucleon numbers up from $N = Z = 20$. Of course, even narrower limits result if the other parameters are kept fixed and/or further details of the shell model spin assignments are required.

5) The i-spin mixing parameter τ determines (like σ) essentially some sort of fine structure; e.g. the isotope shifts in rms radii. Satisfactory fits to most gross data, like masses and radii, are possible with a very wide range of τ values. But in order to fit the isotope mass- as well as rms-dependences and the neutron/proton ratios in heavy nuclei this parameter should be in the range $0.1 < \tau \lesssim 0.5$.

The above discussion reveals the problem of a "fit" here; there are various data of different dimensions that should be reproduced reasonably well. But within the scope of this work there is no obvious selective principle for the preference of a better fit to one particular set of data, say radii, on the expense of fitting other data, masses for example. Naturally, it depends on the application of the model, to which data some sort of least square fit will be performed. In any case, the parameters

should be confined to their "physical" limits discussed above.

The parameter set A of table 1 was used here for the fairly extensive comparison with data of spherical nuclei. The set B of table 1 has the parameters α and ρ_1 close to the limits of their reasonable regions. A decrease in rms radii (by about 4%) that would result due to the increase of ρ_1 from 0.3 to 0.4 fm^{-3} is compensated in this case by increasing the nonlocality from 0.8 to 0.9 fm. Some results for parameter set B are given in table 2.

2.2 Results for a Typical Parameter Set

It should be emphasized that all results in this paper except for table 2 refer to computations done with just the one parameter set A of table 1. I.e. everything is computed with simply the rough center values of the above estimated parameter regions. In view of this fact, the general agreement with data throughout the periodic table is surprisingly good. Absolute values for masses, radii and 1s proton levels are reproduced within a few percent. The mass and radius difference data are quite satisfactorily reproduced, mostly within 30 %. Even the higher order difference quantities like rearrangement energies or isomer radius shifts seem to result with the correct order of magnitude.

Fig. 4 shows density distributions of protons and neutrons (lower and upper solid lines). One point of recent interest is the "neutron skin" of heavy nuclei, [37-40] the Johnson-Teller effect.[41] In the case of ^{208}Pb, for example, the results of pionic scattering and isobaric analog state analyses seem to disagree significantly with mu or K mesic experiments. Rms radius differences of neutron and proton densities deduced from the former type of data are about two percent [37, 40] whereas more than 10 percent are reported from μ^--atoms and K^- capture as well as from some optical and shell model analyses.[38] The present self-consistent model gives rms(n) - rms(p) = 0.07 fm (see table 3) in excellent agreement with the value 0.07 ± 0.03 fm due to an analysis of the isobaric analog state [39] which is consistent with recent $\pi^\pm$-Pb scattering data.[40] In addition, the absolute magnitude of the ^{208}Pb rms charge radius given in table 3 agrees perfectly with elastic electron scattering experiments yielding the value 5.42 ± 0.03 fm.[42] One should notice the neutron skin or halo of ^{208}Pb shown in fig. 4 which looks surprisingly large in view of the small rms radius difference. In the case of ^{40}Ca, the effect is reversed. According to the present calculation, the rms radius of neutrons is 0.04 fm smaller than that of the protons; in qualitative agreement with a recent optical model analysis.[43]

Figure and table 5 give calculated isotopic variations of charge densities for some Sn and Ca isotopes. For example, the calculated ^{44}Ca to ^{40}Ca rms charge radius difference agrees well with experiments.[44] Use of the standard (N-Z)/A term from optical model fits (instead of the term (10)) would yield the wrong sign for this shift.

3. Rearrangement Effects

In any HF-type many-body formalism kernels depend on the occupation functions which are for the ground state e.g. $\theta(\varepsilon_{\nu_{Fermi}} - \varepsilon_\nu)$ in HF or $(1 + (\varepsilon_{\nu_F} - \varepsilon_\nu)/\sqrt{(\varepsilon_{\nu_F} - \varepsilon_\nu) - \Delta^2}\,)/2$ in Hartree-Bogoliubov-type formalisms. The effective force acting on a single nucleon will therefore change when different states (orbits) are occupied by the other particles, i.e. when the residual nucleus rearranges. The corresponding orbital rearrangement energies have been discussed with this model in some detail elsewhere [15]. They were shown to be comparable to eigenvalue-differences in local (Woods-Saxon-type) potential wells. Hence, it is an unjustified simplification to identify such level spacings with the mass differences observed e.g. in nucleon transfer reactions. Parameter set A of table 1 gave a good fit to all difference data in the Ca region. One typical example is the first neutron hole state for ^{47}Ca : The observed mass difference to the ground state of about 2.6 MeV is reproduced by the present single-particle Hamiltonian that gives at least 6 MeV for the corresponding level spacing; i.e. more than 3.4 MeV result from orbital rearrangement (cf. ref. 15).

The agreement with the mass data is also excellent for the ^{40}Ca $\pm$ one nucleon differences (see table 4). For this example another type of rearrangement effect is revealed in fig. 6. Conventionally, the eigenvalues were fitted to the experimental total binding energy differences; i.e. rearrangement was totally neglected. Of course, one could not do better in calculations that had no chance to get the right order of magnitude for the total binding - like in local potential model fits. Here, in fig. 6, the observed binding energy differences are reproduced within 0.2 MeV. However, due to rearrangement, they differ up to 6 MeV from the corresponding eigenvalues.

It might be argued that for some reason this model strongly overestimates rearrangement effects. But the magnitude of this model's rearrangement response can be checked to some extent by a comparison with the calculated isomer shifts due to single-particle excitations (table 6). Their order of magnitude seems to be confirmed by some relevant data [45]. This corroborates the present results on rearrangement energies because of the well-known radial and eigenvalue shift correlation for single-particle potential models.

This observation also casts doubts on shell model calculations that use the observed total binding energy differences (of $A \pm 1$ nucleon systems) as the eigenvalues for one constant single-particle Hamiltonian: Rearrangement destroys the orthogonality of the wave functions for single-particle states of nuclei with different excitations and / or nucleon numbers.

4. The Magic Proton Number 114

The charge spectrum of cosmic ray nuclei indicates the existence of nuclei with $Z \geq 110$ [46]. An increasing amount of experimental effort is spent now to produce such super-heavy nuclei [47]. For some time, $Z = 126$ was the main theoretical candidate for a relatively stable super-heavy nucleus. This belief was based on a simple minded shell model picture that did not differentiate between protons and neutrons and thus assumed a repetition of the $N = 126$ shell in Z.

Shell closures, i.e. structure dependent tendencies to prefer spherical shapes, have been shown to be of prime importance for the spontaneous fission half lifes of super-heavy nuclei [17]. The contribution to the barrier height due to shells is negligible at the proton number $Z = 50$ and is about 30 % of the total for Z around 82 near the beta stability line. In the region beyond $Z = 110$ the average value or liquid-drop-model barrier becomes practically negligible, since it is quite small as compared to the present uncertainties about structure dependent contributions there.

About 4 years ago, calculations of this author showed $Z = 114$, $N = 184$ to be a clearly preferable candidate [16]. This has since been confirmed by many independent computations [14, 18] and is widely discussed now [48]. The extrapolations were based on single-particle potential fits that showed a shell structure in the eigenvalues similar to the one observed in the experimental mass defects. Fluctuating rearrangement effects were totally neglected. Most authors used the questionable procedure of identifying eigenvalue spacings with mass differences (cf. sect. 3).

The present calculations check the real shell effects in the nuclear masses. As can be seen from table 4, the partial derivative $\partial E / \partial Z$ of the total binding energy (mass) changes considerably at the proton number $Z = 114$ when parameter set A of table 1 is used for superheavy nuclei. The present calculations for $N = 172$ and 186 show the expected decrease of the shell effect for isotopes far from the extrapolated beta stability line. At $N = 172$ and $Z = 114$, the lack of neutron excess seems to smoothen the step in the mass function to an insignificant wiggle. For 186 neutrons the shell effect has the magnitude observed at established magic numbers. Therefore, experiments on $Z = 114$ should aim for compound nuclei with mass numbers around 290 or higher.

5. Deformed Nuclei and Fission

It is rather straightforward to extend the model given by eqs. (1), (13) and (14) to nonspherical, in particular axially symmetric density distributions. Present computer sizes, however, seem to require some sort of "local energy approximation" to the nonlocality problem. For this case, most aspects of the resulting numerical work have been investigated recently [49]. The present Hamiltonian is in such an approximation for axial symmetric cases cf. ref. 49, eq. 2.8)

$$H_{m_t} = \frac{\vec{p}^2}{2m} + V(\varepsilon, m_t)\left[1-\left(\frac{\rho_{m_t}(z,b)}{\rho_1}\right)^{\frac{2}{3}}\right]\left[1-\frac{\sigma}{\hbar}(\vec{p}\times\vec{s})\cdot\nabla\right]\rho_{m_t}(z,b) + \left(\frac{1}{2}-m_t\right)V_C(z,b) \qquad (15)$$

where cylinder coordinates (z, b) are introduced, $b^2 = x^2 + y^2$, and is the effective density calculated according to eqs. (13) and (14) . Mainly two methods are used for the computation of the energy dependent local potential that corresponds to a given Van Vleck-type kernel. In bound state calculations the simple technique of using the Fourier transform according to eqs. (4) and (5) ; i.e.

$$V(\varepsilon) = \left[1 + \frac{2m}{\hbar^2}\alpha^2(\varepsilon - V(\varepsilon))\right]^{-1} \qquad (16)$$

is probably as good [50] as the fancier LEA [51]. Equations (15) and (16) give a framework for self-consistent calculations of nuclear single-particle data. The problematic boundary condition of "volume conservation" in equipotential contours, for example, is completely avoided here. In fact all the classical difficulties [52] of the Nilsson-type models for deformed nuclei and adiabatic fission computations do not arise.

6. Conclusions

The final remarks of the proceeding section reveal the main reason for the computations done so far: A check of the qualities of the proposed model that is designed to work for a much wider range of applications. Already here, the proposed Hamiltonian was used for the calculation of more independent data than was conceivable with previous models. For spherical nuclei, one constant set of five physical parameters allowed to reproduce satisfactorily

1) charge density distributions, including isotope and isomar shifts,
2) 1s proton levels as measured in (e, e'p) scattering,
3) total binding energies of nuclear mass defects, and
4) the shell model spin assignments and mass structure

throughout the periodic table. Hence, it seems that all future work in this direction has to confirm quantitatively the essential features of a nuclear kernel determined here; in particular the nonlocality and rearrangement effects. The present concept works quantitatively good enough to allow predictions like the proton shell 114.

Equation (1) was solved (numerically) exactly. The results can therefore be used to check approximations that might be necessary for deformed and fissioning nuclei.

Naturally, there are many improvements to be considered like those mentioned in the discussion about the spin-orbit term. Some residual interaction effects of the pairing type, for instance, could be taken into account by appropriately smoothening the step function used in eq. (14) for the occupation probability distribution.

ACKNOWLEDGEMENTS

I would like to acknowledge the hospitality of the University of California Lawrence Radiation Laboratory and of the U.C. Physics Department. I am indebted to many members of both institutions for helpful discussions. This lengthy investigation would have been impossible without the generous support of Professor S.G. Thompson.

REFERENCES

+ This work was performed under the auspices of the U.S. Atomic Energy Commission while the author was holding a NATO postdoctoral fellowship.

x Present address: Freie Universität Berlin, West-Berlin

1. M.G. Mayer and J.H.D. Jensen, Elementary Theory of Nuclear Shell Structure, John Wiley 1955;
D.H. Wilkinson, Comments on Nuclear and Particle Physics, II, 48 and 83 (1968)

2. H.A. Bethe, Phys. Rev. 103, 1353 (1956)

3. K.A. Brueckner, Phys. Rev. 97, 1353 (1955)

4. cf. E. Lomon and H. Feshbach, Rev. Mod. Phys. 39, 611 (1967)

5. cf. H. Pierre Noyes, SLAC-PUB-256, 1967 (Saclay Conf. paper) et loc. cit. I am indebted to Professor Noyes for enlightning discussions on these problems.

6. cf. e.g. M. L. Goldberger and K. M. Watson, Collision Theory, J. Wiley, N. Y. 1964

7. P.Mittelstaedt and M. Ristig, Z. Phys. 193, 349 (1966), see also G.A. Baker, Phys. Rev. 128, 1485 (1962)

8. S.A. Moszkowski and B.L. Scott, Ann. Phys. (N.Y.) 11, 65 (1960)

9. cf. e.g. the discussion (p. 673) at the International Nuclear Physics Conference at Gatlinburgh, Acad. Press, N.Y. 1967

10. cf. G. Chew, Phys. Rev. Letters 19, 1492 (1967) and Comments on Nuclear and Particle Physics II, 107 (1968)

11. H. Meldner and G. Suessmann, Phys. Letters 6, 353 (1963)

12. A.A. Ross, R.D. Lawson and H. Mark, Phys, Rev. 104, 401 (1956)
P.E. Nemirovsky, JETP (USSR) 9, 627 (1959)
D.J. Wyatt, J.G. Wills and A.E.S. Green, Phys. Rev. 119, 1031 (1960)
L.R.B. Elton and A. Swift, Nucl. Phys. A 94, 52 (1967)

13. H. Meldner, UCRL-16843 (1966) and Arkiv f. Fysik 36, 593 (1967)

14. C. Gustafson, I.L. Lamm, B. Nilsson and S.G. Nilsson, Arkiv f. Fysik 36, 613 (1967)

15. H. Meldner, Nuovo Cim. 53 B, 195 (1968)

16. cf. ref. 23 in the paper of Myers and Swiatecki:

17. W.D. Myers and W.J. Swiatecki, UCRL-11980 (1965) and Nucl. Phys. 81, 1 (1966)

18. A. Sobiczewski, F.A. Gareev and B.N. Kalinkin, Phys. Letters 22, 500 (1966)
S.G. Nilsson, J.R. Nix, A. Sobiczewski, Z. Szymanski, S. Wycech, C. Gustafson and P. Möller, UCRL-18068 (1968) to be published in Nucl. Phys

19. K.T.R. Daries, S.J. Krieger and M. Baranger, Nucl. Phys. 84, 545, (1966)
W.H. Bassichis, A.K. Kerman and J.P. Svenne, Phys. Rev. 160, 746 (1967)
D. Vautherin and M. Véneroni, Phys. Letters, 26B , 552 (1968)
P. Pirès, R. De Tourreil, D. Vautherin and M. Véneroni, 1968 International Symposium on Nuclear Structure , Dubna, USSR
A. Faessler, P.U. Sauer and H.H. Wolter, ibid.

20. For some discussion on this particular choice see e.g.
W.E. Frahn and R.H. Lemmer, Nuovo Cim. 6, 664 (1957)
A.L. Fetter and K.M. Watson in Advances in Theoretical Physics 1, Ed. K.A Brueckner, Acad. Press, N.Y. 1965
A.E.S. Green, Rev. Mod. Phys. 30, 569 (1958)
K.A. Brueckner, Phys. Rev. 103, 1121 (1956)
J.H. Van Vleck, Phys. Rev. 48 , 367 (1935)

21. M.H. Johnson and E. Teller, Phys. Rev. 98, 783 (1955)

V.F. Weißkopf, Nucl. Phys. 3, 423 (1957) and Mod. Phys. 29, 174 (1957)

K.A. Brueckner, A.M. Lockett and M. Rotenberg, Phys. Rev. 121, 255 (1961)

22. U. Amaldi Jr., G.C. Venuti, G. Cortellessa, E. De. Sanctis, S. Frullani, R. Lombard and P. Salvadori, Accad. Naz. Lincei-Rend. Sc. fis. mat. e nat. Serie VIII, vol. XLI, fasc. 6, (results on ^{75}As) and Phys. Letters 22, 593 (1966) (results on ^{40}Ca)

23. G.E. Brown, J.H. Gunn and P. Gould, Nucl. Phys. 46, 598 (1963)

24. P.E. Hodgson, The Optical Model of Elastic Scattering , Oxford Uni. Press (1963)

25. F.G. Perey and B. Buck, Nucl. Phys. 32, 353 (1962)

H. Schulz and H. Wiebicke, Phys. Letters 21, 190 (1966)

26. L. Rosen, J.G. Beery, A.S. Goldhaber and E.H. Auerbach, Ann. Phys. (N.Y.) 34, 96 (1965)

R.L. Cassola and R.D. Koshel, Nuovo Cim. 53 B, 363 (1967)

27. F.G. Perey, Phys. Rev. 131, 745 (1963)

28. cf. e.g. A. Watt, Phys. Letters 27 B, 190 (1968)

29. R.D. Koshel, Phys. Rev. 144, 811 (1966)

30. H.A. Bethe, International Nuclear Physics Conference , Gattinburgh, Acad. Press, N.Y. 1967; see also A. Lande and J.P. Svenne, Phys. Letters 25 B, 91 (1967)

A.M. Green, Phys. Letters 24 B, 384 (1967).

Introducing this term as an explicit density dependence of the two-body potential would modify the relation used here (eq. (18)) for the total binding energy. - I am grateful to Professor K.A. Brueckner for discussions on these questions.

31. A.M. Lane, Nucl. Phys. 35, 676 (1962)

32. B.F. Gibson and K.J. van Oostrum, Nucl. Phys. 90 A , 159 (1967)

cf. also A. Swift and L.R.B. Elton, Phys. Rev. Letters 17, 484 (1966)

33. P.C. Sood and H.G. Leighton, Nucl. Phys. 111 A, 209 (1968)

34. K.A. Brueckner, J.L. Gammel and H. Weitzner, Phys. Rev. 110, 431 (1958)

35. J.B. Law and D.W.L. Sprung, 1968 International Symposium on Nuclear Structure, Dubna, USSR

36. cf. e.g. V.A. Chepurnov and P.E. Nemirovsky, Nucl. Phys. 49, 90 (1963)

37. D.H. Wilkinson, 1968 International Symposium on Nuclear Structure, Dubna, USSR and Comments on Nuclear and Particle Physics I, 80 (1967)

38. L.R.B. Elton, Phys. Letters 26 B, 689 (1968)

G.W. Greenless, G.S. Pyle and Y.C. Tang, Phys. Rev. Letters 17, 33 (1968)

B. Holmquist and T. Wiedling, Phys. Letters 27 B, 411 (1968)

H.A. Bethe and P.J. Siemens, Phys. Letters 27 B, 549 (1968)

39. S.A. Nolen Jr., J.P. Schiffer and N. Williams, Phys. Letters 27 B, 1 (1968)

40. E. H. Auerbach, H.M. Querski and M.M. Sternheim, Phys. Rev. Letters 21, 162 (1968)

41. cf. M.H. Johnson and E. Teller, Phys. Rev. 93, 357 (1954)

42. J. Bellicard and K.J. van Oostrum, Phys. Rev. Letters 19, 242 (1967)

43. N. Berovic, P.M. Rudolph and S.M. Scarott, Phys. Letters 27 B, 477 (1968)

44. K.J. van Oostrum, R. Hofstadter, G.K. Nöldecke, M.R. Yearian, B.C. Clark, R. Herman and D.G. Ravenhall, Phys. Rev. Letters 16, 528 (1966)

R.D. Ehrlich, D. Fryberger, D.A. Jensen, C. Nissim-Sabat, R.J. Powers, V.L. Telegdi and C.K. Hargrove, Phys. Rev. Letters 18, 959 (1967)

45. D. Quitmann, UCLRL Berkeley, private communication

46. P.H. Fowler, University of Bristol, Wills Phys. Lab. preprint.
I am grateful to Professor N. Flerov for drawing my attention to this work.

47. S.G. Thompson, UCLRL Berkeley, private communication

N. Flerov, 1968 International Symposium on Nuclear Structure, Dubna, USSR

48. A.M. Weinberg, Physics Today 20, No. 6, 23 (1967); C.Y. Wong, Phys Rev. Letters 19, 328 (1967
see also Session on Super-Heavy Nuclei, 1968 Int. Symp. Nucl. Struct., Dubna USSR

49. F. Dickmann, Zeits. Phys. 203, 141 (1967)

50. M. Krell, Zeits. Phys. 205, 272 (1967)

51. cf. e.g. H. Meldner and G. Suessmann, Zeits. Naturf. 20 a, 1217 (1965)
H. Fiedeldey, Nucl. Phys. 77, 149 (1966)

52. L. Wilets, Theories of Nuclear Fission, chapter 4.3, Clarendon Press, Oxford 1964

53. e.g. the Fortran routine LINIT of the UCLRL Berkeley Computing Center

54. H. Wielandt, Bestimmung höherer Eigenwerte durch gebrochene Iteration, Ber. B 44/J/37, Aerodyn. Vers.-Anstalt Göttingen 1944,

J.H. Wilkinson, The Algebraic Eigenvalue Problem, p. 321, Clarendon Press, Oxford 1965

55. G.N. Watson, Theory of Bessel Functions, Uni. Press Cambridge 1962

56. F. Burmiller, M. Croissiaux, E. Dally and R. Hofstadter, Phys. Rev. 124, 1623 (1961) for a comparison with other formfactors see P. Hofstadter, Rev. Mod. Phys. 30, 482 (1958)

57. P.E. Nemirovsky and Yu. V. Adamchuck, Nucl. Phys. 39, 551 (1962)

58. D. Quitmann, Zeits. Phys. 206, 113 (1967)

APPENDIXES

For spherical symmetric density distributions the radial equation is

$$\left[\frac{\hbar^2}{2m}\left(\frac{d^2}{dr^2} - \frac{\ell(\ell+1)}{r^2}\right) - \varepsilon_{n\ell j m_t}\right] u_{n\ell j m_t}(r) =$$

$$v\int_0^\infty dr' h_\ell(r,r')\left[1-\left(\frac{\rho_{m_t}(x)}{\rho_1}\right)^{\frac{2}{3}}\right]\cdot\left[\rho_{m_t}(x) - \frac{\sigma}{2x}\left(j(j+1)-\ell(\ell+1)-\frac{3}{4}\right)\rho'_{m_t}(x)\right] u_{n\ell j m_t}(r') \quad (17)$$

$$+\left(\frac{1}{2}-m_t\right)\frac{Z-1}{Z}e^2\left[\frac{1}{r}\int_0^r dr' r'^2 \rho_{(-\frac{1}{2})}(r') + \int_r^\infty dr' r' \rho_{(-\frac{1}{2})}(r')\right] u_{n\ell j m_t}(r)$$

where $x = \frac{r+r'}{2}$; n denotes the radial, ℓ the orbital angular momentum, j the total angular momentum quantum number, and m_t the i-spin 3-component for the nucleon in question; ρ' is the derivative of ρ with respect to the argument and $e^2 = 1.4368$ MeVfm. The h_ℓ are the partial wave projections of the width-function $v(|\vec{r} - \vec{r}'|)$.

The single-particle equation is assumed to emerge from pure two-body internucleon forces. The total binding energy is therefore

$$E = \sum_i t_i - \frac{1}{2}\sum_{i,j} u_{ij} = \frac{1}{2}\sum_i \left[\varepsilon_i + \int d\vec{r}\, \varphi_i^*(\vec{r})\, t(\vec{r})\, \varphi_i(r)\right] \quad (18)$$

where the sums extend over the occupied levels; t_i is for the spherical cases

$$t_{n\ell j m_t} = \frac{\hbar^2}{2m}\int_0^\infty dr\left[\frac{\ell(\ell+1)}{r^2} u^2_{n\ell j m_t}(r) + \left(r\frac{d}{dr}\frac{u_{n\ell j m_t}(r)}{r}\right)^2\right] \quad (19)$$

A1. Eigenstates in Strongly Nonlocal Potentials

The computer problem is to find the first few eigenvalues e and eigenvectors u of an integro-differential equation

$$\left[\frac{d^2}{dr^2} - (e+C(r))\right] u(r) + \int_0^\infty dr' g(r,r') u(r') = 0 \qquad (20)$$

for boundary conditions of the type $\lim_{r\to 0} u(r) \sim r^{\ell+1}$ and $\lim_{r\to\infty} u(r) \sim \exp(-r\sqrt{e})$. Selecting an appropriate finite integration interval $(0, R)$, divided into N parts and with $s = R/N$, $c_i := C(is)$, and $g_{ij} := g(is, js)$ one gets the corresponding difference equation $(h - e)\, u = 0$ with a symmetric matrix

$$h = \begin{pmatrix} sg_{11} - C_1 - \frac{2}{s^2} & sg_{12} + \frac{1}{s^2} & sg_{13} & \cdots & sg_{1N} \\ sg_{21} + \frac{1}{s^2} & sg_{22} - C_2 - \frac{2}{s^2} & & & \\ sg_{31} & & & & \\ & & & & \\ & & & & \\ sg_{N1} & & & & sg_{NN} - C_N - \frac{2}{s^2} \end{pmatrix}$$

A good approximation $u^{(0)}$ to u is obtained e.g. from a LEA program [51]. The vector $u^{(0)}$ fulfills approximately the same boundary conditions as u and has the same number of nodes. An appropriate iteration program is:

i : = 0

[1] nomalize $u^{(i)} := u^{(i)} \frac{1}{u^{(i)T} u^{(i)}}$

[2] compute $e^{(i)} = u^{(i)T} h\, u^{(i)}$

[3] solve $u^{(i+1)} = (h - e^{(i)})^{-1} u^{(i)}$ with some standard inversion program [53]

[4] i : = i + 1, go to [1] until $|e^{(i+1)} - e^{(i)}| / |e^{(i)}| \ll 1$

This "Wielandt Inverse Iteration" [54] works as follows: Let v be the exact solution, i.e. $(h - e_m)\, v_m = 0$. Then, step [3] is in spectral decomposition

$$\sum c_m^{(i+1)} v_m = (h - e_n^{(i)})^{-1} \sum c_m^{(i)} v_m = \sum_m \frac{c_m^{(i)}}{e_m - e_n^{(i)}} v_m \,, \qquad (21)$$

$$\text{i.e.} \quad c_m^{(i+1)} = \frac{c_m^{(i)}}{e_m - e_n^{(i)}} \,.$$

Therefore, the iteration converges to the nearest eigenvector v_m which is picked out via the above pole.

A2. Partial Wave Projections of Yukawafunctions

The above h_1 are $h_\ell(r,r') = 2\pi rr' \int_{-1}^{1} dz\, P_\ell(z) \frac{\exp(-|\vec{r}-\vec{r}'|/a)}{|\vec{r}-\vec{r}'|/a}$

with $r = |\vec{r}|, \quad z = \frac{\vec{r}\vec{r}'}{rr}$

since [55] $\frac{\exp\left(-\frac{1}{a}\sqrt{r^2+r'^2-2rr'z}\right)}{\sqrt{r^2+r'^2-2rr'z}} = \sum_{\ell=0}^{\infty} (2\ell+1) P_\ell(z) \frac{1}{\sqrt{rr'}} K_{\ell+\frac{1}{2}}\left(\frac{r'}{a}\right) I_{\ell+\frac{1}{2}}\left(\frac{r}{a}\right)$

i.e. $h_\ell(r,r') = 4\pi a \sqrt{rr'}\, I_{\ell+\frac{1}{2}}\left(\frac{r}{a}\right) K_{\ell+\frac{1}{2}}\left(\frac{r'}{a}\right)$ for $r<r'$

and also from ref. 55, p. 80

$$I_{\ell+\frac{1}{2}}(x) K_{\ell+\frac{1}{2}}(x') = \frac{1}{2\sqrt{xx'}} \left[e^{x} \sum_{k=0}^{\ell} (-)^k T_{\ell k}(x) - (-)^\ell e^{-x} \sum_{k=0}^{\ell} T_{\ell k}(x)\right] e^{-x'} \sum_{k=0}^{\ell} T_{\ell k}(x')$$

with $T_{\ell k}(x) = \frac{(\ell+k)!}{k!\,(\ell-k)!\,(2x)^k}$

the following formula is feasible for computations:

$$h_\ell(r,r') = 2\pi a^2 \left[e^{\frac{r}{a}} \sum_{k=0}^{\ell} (-)^k T_{\ell k}\left(\frac{r}{a}\right) - (-)^\ell e^{\frac{r}{a}} \sum_{k=0}^{\ell} T_{\ell k}\left(\frac{r}{a}\right)\right] e^{-\frac{r'}{a}} \sum_{k=0}^{\ell} T_{\ell k}\left(\frac{r'}{a}\right) \text{ for } r<r' \quad (22)$$

i.e. $h_0(r,r') = 2\pi a^2 \left(e^{\frac{r}{a}} - e^{-\frac{r}{a}}\right) e^{-\frac{r'}{a}}$ etc.

A3. Charge Density and Proton Formfactors

The nuclear charge density ρ_{ch} is obtained by folding the proton probability distribution with the electric proton formfactor f

$$\rho_{ch}(\vec{r}) = \sum_{\nu}^{\nu_F} \int d\vec{r}' |\varphi_{\nu,-\frac{1}{2}}|^2 f(|\vec{r}-\vec{r}'|) \tag{23}$$

The $\varphi_{\nu,-\frac{1}{2}}$ are properly normalized single-particle wave functions and the sum extends over all occupied proton levels. The best phenomenological proton formfactor appears to be an exponential [56]:

$$f(r) = \frac{\alpha^3}{8\pi} \exp(-\alpha r) \qquad \text{with} \quad \alpha = \sqrt{\frac{12}{\langle r^2 \rangle}} \quad \text{and} \quad \langle r^2 \rangle = \int d\vec{r}\, r^2 f(r)$$

For spherical symmetric $\rho = \sum |\varphi|^2$ one has

$$\rho_{ch}(r) = 2\pi \int_0^\infty dr' r'^2 \rho(r') \int_{-1}^{1} dz\, f\left(\sqrt{r^2+r'^2-2rr'z}\right)$$

which is here

$$\rho_{ch}(r) = \frac{\alpha}{4r} \int_0^\infty dr' r' \rho(r') \left[(\alpha|r-r'|+1) e^{-\alpha|r-r'|} - (\alpha(r+r')+1) e^{-\alpha(r+r')} \right] \tag{24}$$

The present calculations were done with the value $\langle r^2 \rangle$ = 0.75 fm (cf. ref. 56).

Table 1. The two parameter sets used in the present calculation. Except for table 2 all results refer to parameter set A.

	v/MeV	a/fm	ρ_0/fm	σ/fm	τ
set A	391.3	0.8	0.3	0.5	0.3
set B	289.0	0.9	0.4	0.5	0.3

Table 2. Some results for parameter set B; cf. sect. 2.1. For experimental data and the pairing correction see tables 3 and 4.

	Binding Energy/MeV	$\langle r^2 \rangle^{\frac{1}{2}}_{\text{charge}}$/fm
^{44}Ca	396.4	3.18
^{208}Pb	1636.2	5.38
^{209}Bi- ^{208}Pb	4.9	
^{208}Pb- ^{207}Tl	5.7	
^{209}Pb- ^{208}Pb	4.8	
^{208}Pb- ^{207}Pb	5.3	

Table 3. Binding energies and rms radii for some spherical nuclei.

Additional comparisons with experimental data give e.g. 1 s proton level in ^{40}Ca: experimental 77±14 MeV [22], calculated 79 MeV.

Nucleus	Binding Energy/MeV		Calculated rms radii/fm		
	Exp.	Calc.	$\langle r^2 \rangle^{\frac{1}{2}}_{\text{charge}}$	$\langle r^2 \rangle^{\frac{1}{2}}_{p}$	$\langle r^2 \rangle^{\frac{1}{2}}_{n}$
^{40}Ca	342.0	339.4	3.15	3.06	3.02
^{44}Ca	380.9	380.3	3.22	3.13	3.20
^{48}Ca	416.1	426.6	3.29	3.20	3.34
^{88}Sr	768.5	777.5	4.02	3.95	4.02
^{118}Sn	1004.8	1017.9	4.50	4.43	4.47
^{140}Ce	1172.8	1189.0	4.47	4.68	4.73
^{208}Pb	1636.4	1636.4	5.44	5.38	5.45
^{300}114		2140.5	6.26	6.21	6.24

UCRL-17801

Table 4. Rms radius and binding energy differences at closed shells $\pm$ one nucleon for established magic numbers and for $Z = 114$.

Magic Number	Nuclei	Binding Energy Differences/MeV Exp.	Calc.	Calc. Radius Differences/fm $\Delta\langle r^2\rangle^{\frac{1}{2}}_p$	$\Delta\langle r^2\rangle^{\frac{1}{2}}_n$
N = 20	$^{41}Ca - ^{40}Ca$	8.4	8.4	0.019	0.048
	$^{40}Ca - ^{39}Ca$	15.6	15.3	0.006	0.005
Z = 20	$^{41}Sc - ^{40}Ca$	1.1	1.1	0.051	0.022
	$^{40}Ca - ^{39}K$	8.3	8.0	0.021	0.011
N = 28	$^{49}Ca - ^{48}Ca$	5.0	0	0.010	0.042
	$^{48}Ca - ^{47}Ca$	10.1	13.3	0.020	0.034
Z = 28	$^{63}Cu - ^{62}Ni$	6.1	2.7	0.011	0.003
	$^{62}Ni - ^{61}Co$	11.1	13.9	0.033	0.017
N = 50	$^{89}Sr - ^{88}Sr$	6.8	5.3	0.007	0.013
	$^{88}Sr - ^{87}Sr$	11.1	11.7	0.004	-
Z = 50	$^{119}Sb - ^{118}Sn$	5.2	2.3	0.008	-
	$^{118}Sn - ^{117}In$	9.9	10.7	0.004	-

table 4 cont.

N = 82	$^{141}Ce - ^{140}Ce$	5.5	3.3	-	0.007
	$^{140}Ce - ^{139}Ce$	9.1	8.6	0.005	-
Z = 82	$^{209}Bi - ^{208}Pb$	3.8	3.3	0.008	-
	$^{208}Pb - ^{207}Tl$	8.0	5.5	-	-
N = 126	$^{209}Pb - ^{208}Pb$	3.9	3.2	0.004	-
	$^{208}Pb - ^{207}Pb$	7.4	5.4	0.004	0.006
Z = 114	$^{287}115 - ^{286}114$	-	0	-	-
	$^{286}114 - ^{285}113$	-	3.4	-	-
	$^{301}115 - ^{300}114$	-	0.1	-	-
	$^{300}114 - ^{299}113$	-	5.2	-	-

The pairing correction is assumed to be $15/A^{\frac{1}{2}}$MeV [57]. For experimental rms charge radius differences cf. e.g. ref. 58. The energies are calculated with an accuracy of about 0.2 MeV, the radii within about $3 \cdot 10^{-3}$ fm. No radius difference is reported for cases where the result was smaller than this error. The calculated charge radius differences agree with the corresponding proton results within the numerical accuracy.

Table 5. Some calculated isotope shifts of rms radii.

	$\Delta\langle r^2\rangle_p^{\frac{1}{2}}$/fm	$\Delta\langle r^2\rangle_n^{\frac{1}{2}}$/fm
$^{44}Ca - ^{40}Ca$	0.08	0.08
$^{48}Ca - ^{44}Ca$	0.08	0.15
$^{120}Sn - ^{118}Sn$	0.04	0.06
$^{114}Sn - ^{112}Sn$	0.01	0.01

Within the accuracy of the calculation the charge radius differences are equal to the corresponding proton results and the $^{124\text{-}122}Sn$, $^{122\text{-}120}Sn$, $^{118\text{-}116}Sn$ as well as the $^{116\text{-}114}Sn$ differences are all equal to the $^{120\text{-}118}Sn$ shift . Note the large calculated neutron rms radius difference for $^{48\text{-}44}Ca$.

Table 6. Examples of rms charge radius differences between the first one neutron hole excitation and the ground state. Except for the case of Ca, the amount of computer time invested here did not allow to check for more than the orders of magnitude.

	$\Delta\langle r^2\rangle_p^{\frac{1}{2}}$/fm	$\Delta\langle r^2\rangle_n^{\frac{1}{2}}$/fm
$^{47}Ca - {}^{47}Ca$	0.012	0.037
$^{207}Tl - {}^{207}Tl$	10^{-3}	10^{-3}
$^{207}Pb - {}^{207}Pb$	10^{-4}	10^{-3}

FIGURE CAPTIONS

Fig. 1 Depth of the nucleon- nucleus potential as function of energy. The solid bars give the limits for regions 1 to 4 as discussed in sect. 1.1 .

Fig. 2 Proton eigenvalue spectra for spherical nuclei close to the line of beta stability. Eigenvalues with equal quantum numbers are connected by straight lines (to guide the eye). Note the somewhat fluctuating results as compared to the smooth curves of non-self-consistent calculations [13] .

Fig. 3 Neutron eigenvalue spectra ; cf. fig. 2 .

Fig. 4 Upper and lower solid curves give the density distributions of protons and neutrons for some nuclei on the beta stability line. The dashed curves are the nuclear charge densities calculated with eq. (24) from the corresponding (bare) proton densities. Examples of Fermi function fits to electron scattering data are shown as dotted curves. The different fits of ref. 44 are practically indistinguishable in this figure.

Fig. 5 Isotopic variation of charge density distributions for ^{40,44,48}Ca and ^{112,118,124}Sn; cf. table 5 for rms radii.

Fig. 6 Example for rearrangement effects: N = Z = 20 shell $\pm$ one nucleon. Compare the eigenvalues/MeV (arrows) with the circled total binding energy differences Δ E/MeV. An excellent fit to the data results (cf. table 4) when a pairing correction of 2.4 MeV is added to ^{40}Ca. Conventionally, the eigenvalues are identified with total binding energy differences; cf. sect. 3 .

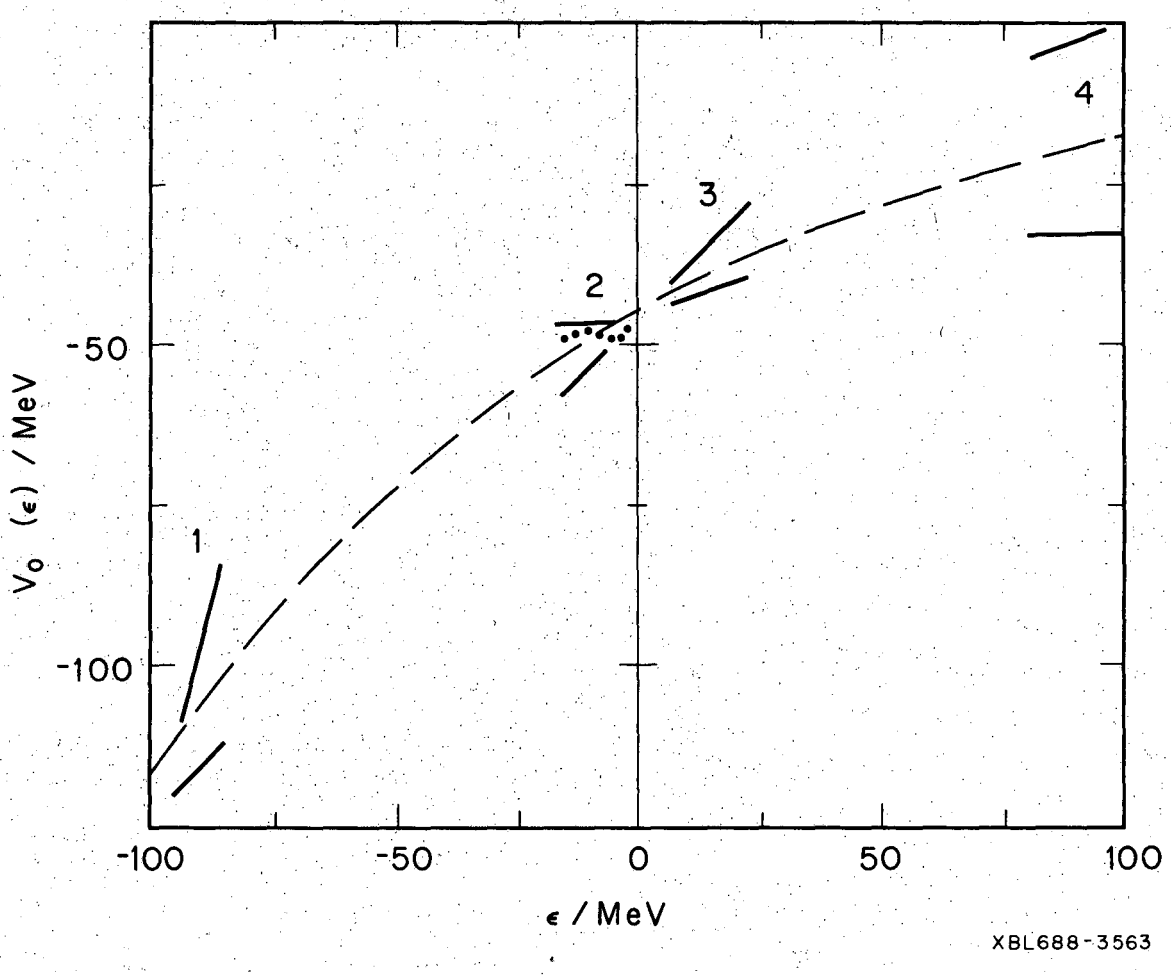
1
2
3
4
-50
-100
V_o (ϵ) / MeV
-100
-50
0
50
100
ϵ / MeV
XBL688-3563

Fig. 1

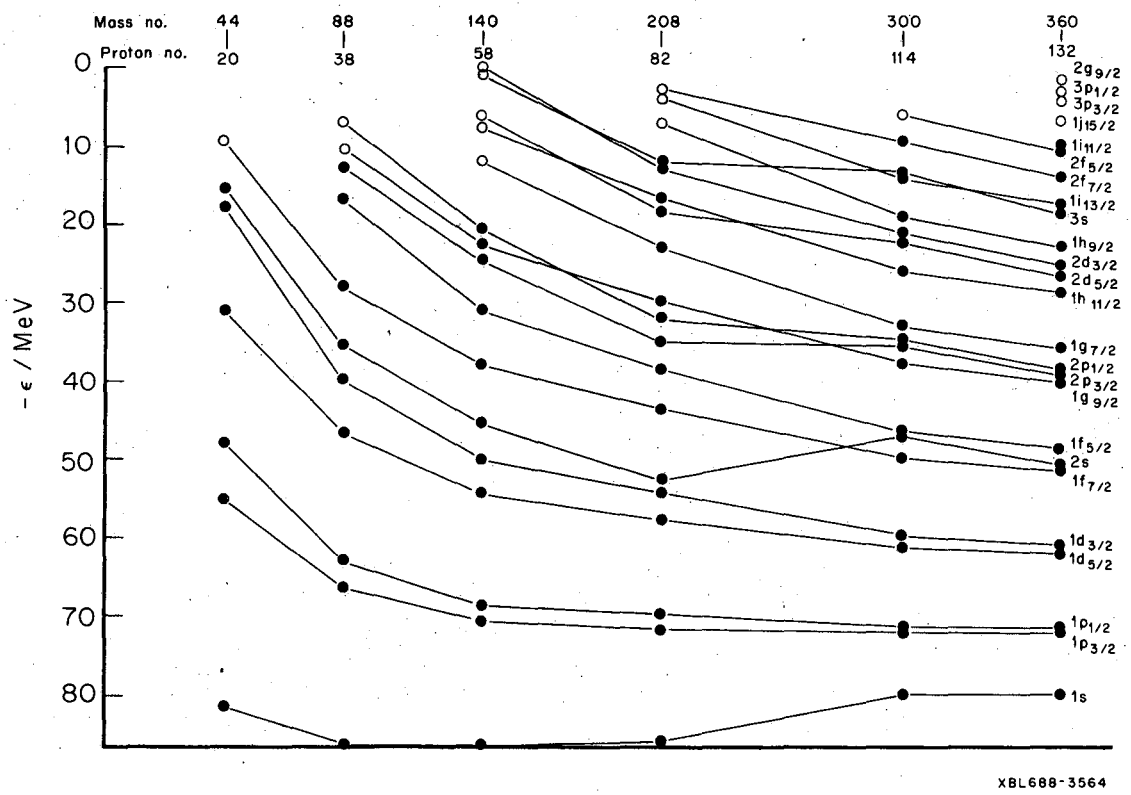
Mass no.
Proton no.
44
20
88
38
140
58
208
82
300
114
360
132
0
10
20
30
40
50
60
70
80
-ε / MeV
2g9/2
3p1/2
3p3/2
1j15/2
1i11/2
2f5/2
2f7/2
1i13/2
3s
1h9/2
2d3/2
2d5/2
1h11/2
1g7/2
2p1/2
2p3/2
1g9/2
1f5/2
2s
1f7/2
1d3/2
1d5/2
1p1/2
1p3/2
1s
XBL688-3564

Fig. 2

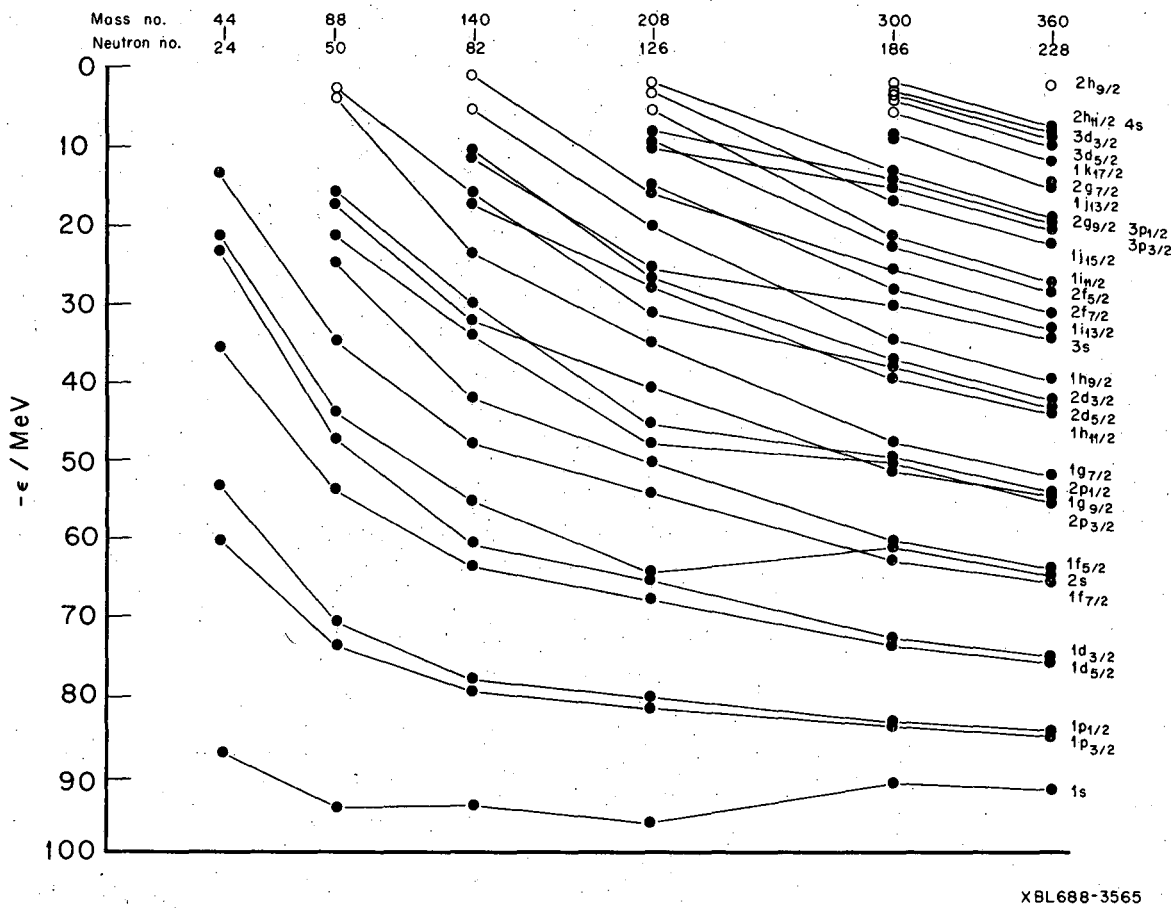
Mass no.
Neutron no.
44
24
88
50
140
82
208
126
300
186
360
228
0
10
20
30
40
50
60
70
80
90
100
-ε / MeV
2h9/2
2hll/2 4s
3d3/2
3d5/2
1k17/2
2g7/2
1j13/2
2g9/2 3p1/2
3p3/2
1j15/2
1i11/2
2f5/2
2f7/2
1i13/2
3s
1h9/2
2d3/2
2d5/2
1hll/2
1g7/2
2p1/2
1g9/2
2p3/2
1f5/2
2s
1f7/2
1d3/2
1d5/2
1p1/2
1p3/2
1s
XBL688-3565

Fig. 3

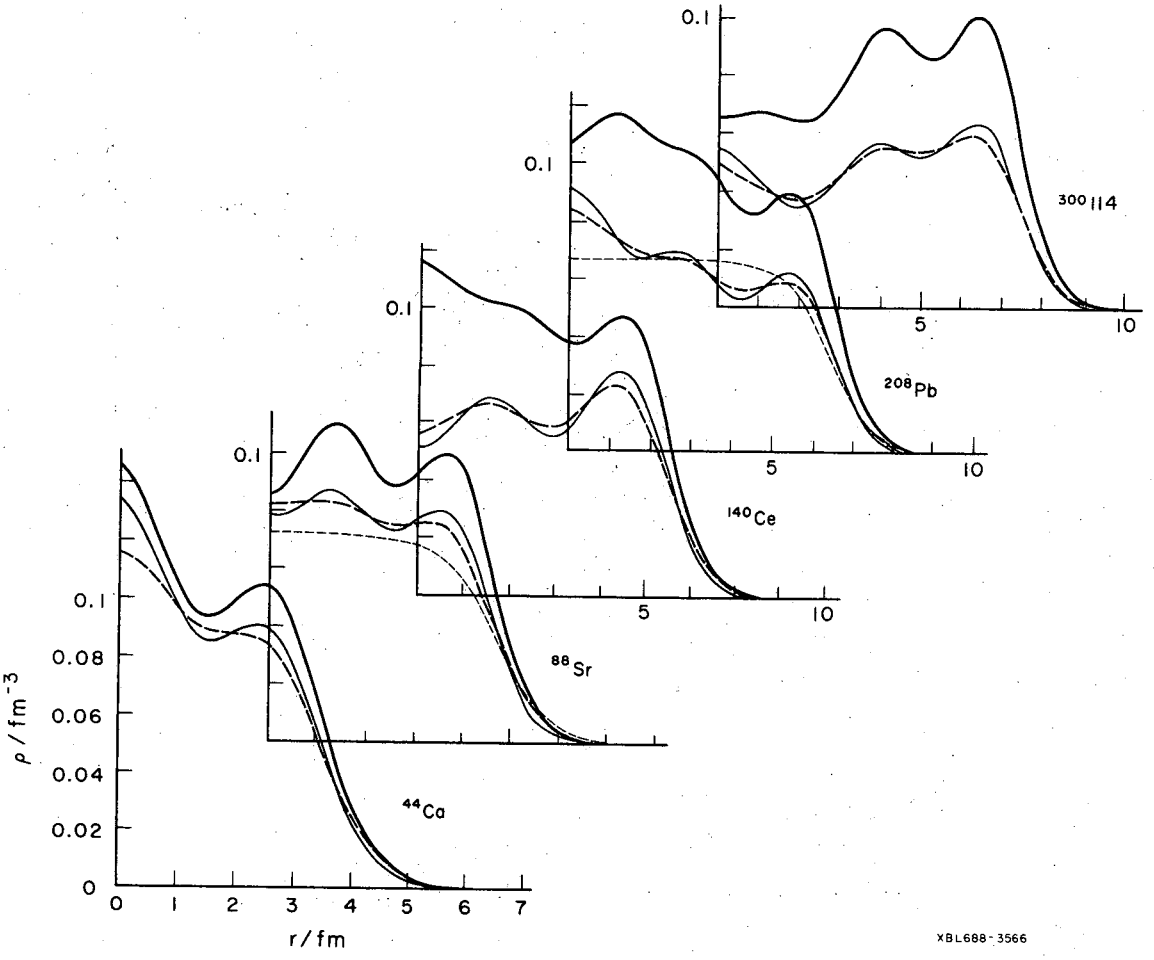
0.1
0.1
0.1
0.1
$^{300}114$
^{208}Pb
^{140}Ce
^{88}Sr
^{44}Ca
5
10
0.1
0.08
0.06
0.04
0.02
0
ρ / fm^{-3}
0 1 2 3 4 5 6 7
r / fm
XBL688-3566

Fig. 4

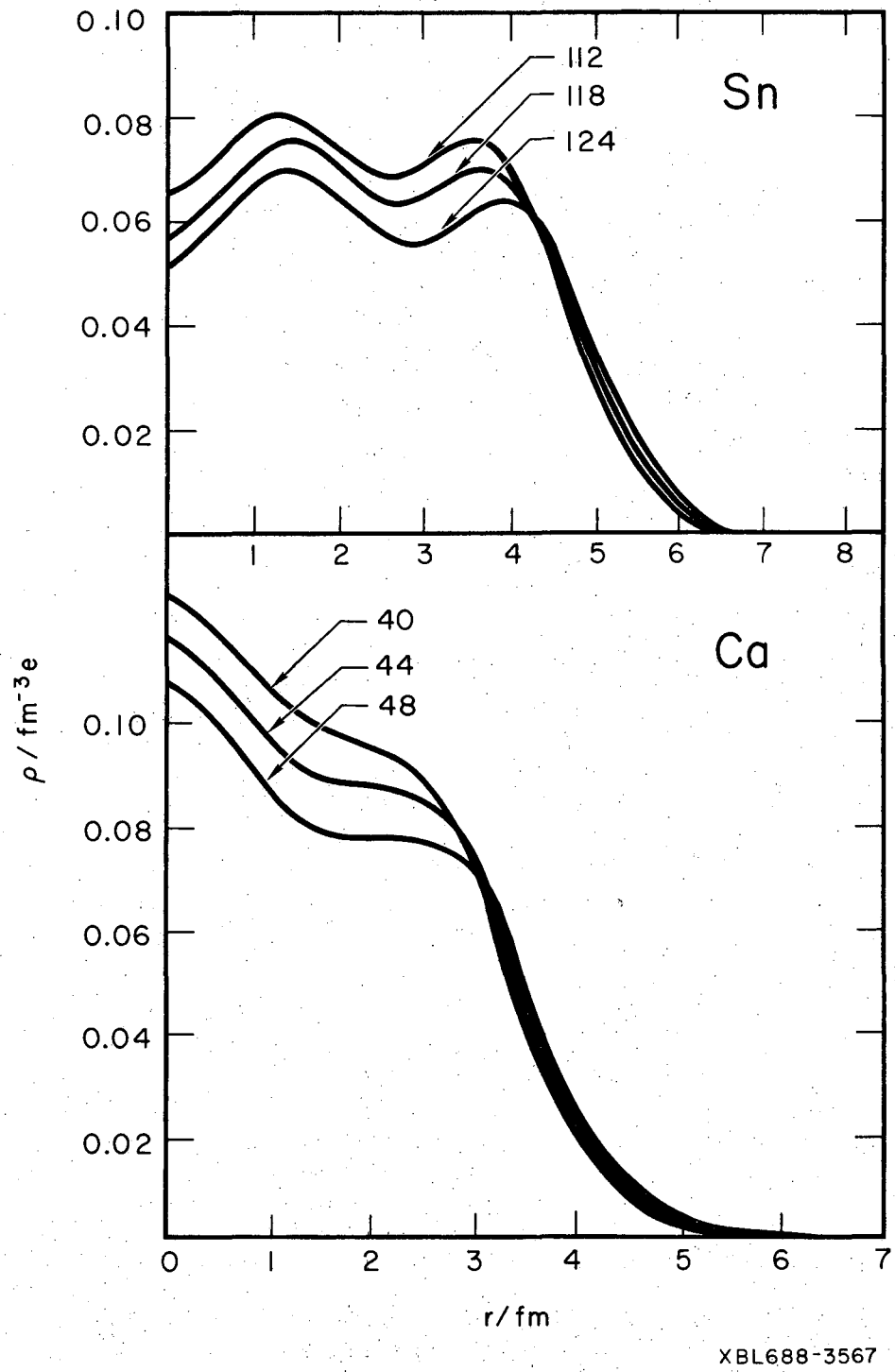
0.10
0.08
0.06
0.04
0.02
112
118
124
Sn
1
2
3
4
5
6
7
8
40
44
48
Ca
ρ / fm⁻³e
0.10
0.08
0.06
0.04
0.02
0
1
2
3
4
5
6
7
r/fm
XBL688-3567

Fig. 5

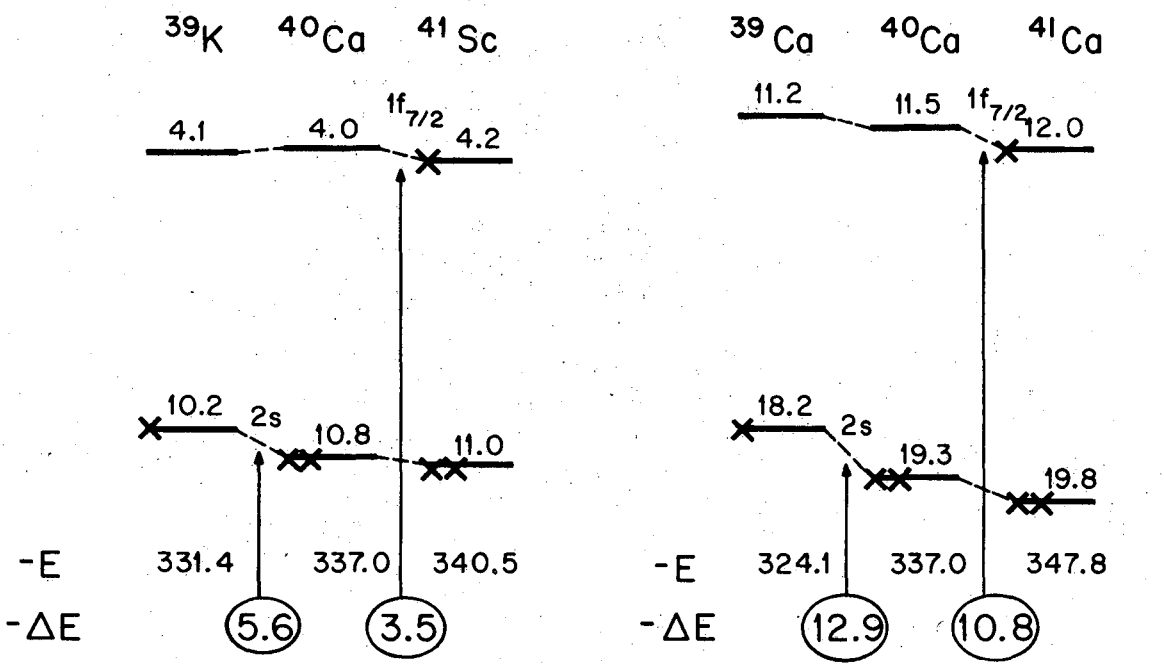

XBL-688-3568

Fig. 6

TECHNICAL INFORMATION DIVISION
LAWRENCE RADIATION LABORATORY
UNIVERSITY OF CALIFORNIA
BERKELEY, CALIFORNIA 94720